Article

Cite This: *Biomacromolecules* 2018, 19, 4593−4606

pubs.acs.org/Biomac

Crystallization Inhibition Properties of Cellulose Esters and Ethers for a Group of Chemically Diverse Drugs: Experimental and Computational Insight

Laura I. Mosquera-Giraldo,[†] Carlos H. Borca,[‡] Andrew S. Parker,[§] Yifan Dong,[∥] Kevin J. Edgar,[⊥] Stephen P. Beaudoin,[§] Lyudmila V. Slipchenko,[‡] and Lynne S. Taylor*[,†]

[†]Department of Industrial and Physical Pharmacy, College of Pharmacy, Purdue University, West Lafayette, Indiana, United States

[‡]Department of Chemistry, College of Science, Purdue University, West Lafayette, Indiana, United States

[§]Department of Chemical Engineering, College of Engineering, Purdue University, West Lafayette, Indiana, United States

[∥]Department of Chemistry, College of Science, Virginia Tech, Blacksburg, Virginia, United States

[⊥]Department of Sustainable Biomaterials, College of Natural Resources and Environment, Virginia Tech, Blacksburg, Virginia, United States

Supporting Information

ABSTRACT: Amorphous solid dispersions are widely used to enhance the oral bioavailability of poorly water-soluble drugs. Polymeric additives are commonly used to delay crystallization of the drug from the supersaturated solutions formed upon ASD dissolution by influencing the nucleation and growth of crystals. However, there is limited evidence regarding the mechanisms by which polymers stabilize supersaturated drug solutions. The current study used experiments and computational modeling to explore polymer−drug interactions in aqueous solutions. Nucleation induction times for supersaturated solutions of nine drugs in the presence of five newly synthesized cellulose-based polymers were evaluated. The polymers had carboxylic acids substituents with additional variations in the side-chain structure: (1) one with a single side chain and a carboxylic acid termination, (2) three with a branched side chain terminated with a carboxylic and an alcohol group (varying the cellulose linkage and the length of the hydrocarbon side chain), and (3) one with a branched side chain with two carboxylic acid end groups. The polymers with a short side chain and one carboxylic acid were effective, whereas the polymers with the two carboxylic acids or a long hydrocarbon chain were less effective. Atomic force microscopy experiments, evaluating polymer adsorption onto amorphous drug films, indicated that the effective polymers were uniformly spread across the surface. These results were supported by molecular dynamics simulations of a polymer chain in the presence of a drug aggregate in an aqueous environment, whereby the effective materials had a higher probability of establishing close contacts and more negative estimated free energies of interaction. The insights provided by this study provide approaches to design highly effective polymers to improve oral drug delivery.

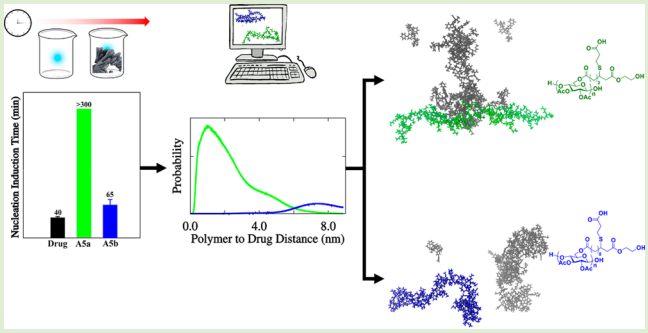

INTRODUCTION

Molecular modeling has provided crucial assistance to the discovery of new drug candidates in recent years.[1−4] Integrating modeling at the discovery stage allows researchers to anticipate which chemical structures will provide superior interactions with target proteins. The most promising drug candidates are synthesized and then tested for drug activity using high throughput screening experiments.[1] The use of computational modeling during these early stages has been supported by the availability of protein crystal structures, the fast development of computing capabilities, and the design and implementation of new methodologies to determine protein−ligand interaction energies.[5]

Optimization of drug candidates to enhance biopharmaceutical properties is essential, and significant effort is devoted to improve their aqueous solubility.[6] Most of the strategies to increase drug solubility involve the use of additional components, namely excipients, which interact with drug molecules and influence in vivo performance of the final drug formulation. These components include surfactants, cyclodextrins, polymers, and cosolvents.

Amorphous solid dispersions (ASD) are one solubilization strategy that enables the creation of supersaturated solutions, whereby the drug concentration exceeds the equilibrium crystalline solubility in a given medium. Polymers are added to

Received: August 23, 2018
Revised: October 26, 2018
Published: October 30, 2018

DOI: 10.1021/acs.biomac.8b01280
Biomacromolecules 2018, 19, 4593−4606

kinetically stabilize the amorphous solid formulation and maintain supersaturation for biorelevant time periods. However, variations in the chemical structure of polymers drastically influence their ability to delay crystallization from supersaturated solutions.[7,8] This leads to two important questions in the field: (1) what chemical functionalities are important for effective polymeric excipients for amorphous solid dispersion drug delivery and (2) what role do these chemical functionalities play.

The use of novel synthetic approaches has allowed the creation of promising polymers for ASDs, also providing information about structural features important for effective crystallization inhibitors.[7−15] The polymers investigated to date can be divided into two groups: synthetic copolymers, and cellulose-based polymers, and have been mainly inspired by the polymers used in commercial ASD formulations.

Computational modeling approaches are helpful to explore how variations in polymer chemical structure can influence their tendency to self-interact and to interact with drug molecules. Numerous computational chemistry studies for drug-polymer systems have been reported recently. Simulations offer molecular insight when experimental information is limited.[16−27] There are various types of computational methods applicable to chemical systems. However, the choice will depend on the problem, the properties of interest, and the size of the model system.

Gas-phase quantum-chemical calculations of monomer−drug binding energies have been one of the most common approaches to study drug−polymer interactions.[17,28,29] Atomistic and coarse-grained dynamics have also been used to study larger systems.[16,21−25,30,31] Some of these studies have aimed to grasp the mechanism of incorporation of drug molecules into polymeric carriers for nanoparticle drug delivery systems. The enthalpy of mixing is determined and subsequently used for calculation of the Flory−Huggins interaction parameter, which offers an indication of drug−polymer miscibility.[21,23]

There are limitations as to the types of conclusions that can be drawn from the current methodologies to calculate monomer−drug binding energies. First, typically the type of conformations chosen accentuate certain intermolecular interactions believed to be relevant, such as hydrogen bonding, but a broad range of drug−polymer conformations are expected in ASDs. Second, intermolecular drug-polymer hydrogen bonds are probably largely disrupted once an ASD encounters an aqueous environment, and other interactions may become more critical. Third, quantum mechanical calculations are limited to small systems, for example, monomers and dimers, due to high computational costs. It is debatable whether the conformations and interaction energies obtained from monomer−drug model systems are representative of the real system, in which oligomers or polymers are present. Fourth, most of these simulations are conducted in the gas phase, but conformations found in real-life solvent systems may differ from these.

Atomistic molecular dynamics (MD) studies in this field demonstrate that modeling could be used to calculate thermodynamic variables and assist in the process of determining how favorable interactions are between two or more components.[21,23] Furthermore, recent combined experimental and computational studies in the area of ASDs have shown promise.[7]

Herein, we hypothesize that a multifaceted approach can be employed to elucidate chemical features important for polymeric crystallization inhibitors. We test this hypothesis by synthesis of new cellulose-based polymers, measurement of their crystallization inhibition properties against a carefully selected group of nine drugs and estimation of polymer−drug interactions. The polymers explored are cellulose ethers and esters with carboxylic acid functionalities, as displayed in Figure 1 and described in Table 1. The experimental measurements involve the determination of crystallization induction times, and the analysis of polymer adsorption on amorphous films of the drug, using atomic force microscopy (AFM). The computational approach consists in estimating free energies of polymer−drug interactions, as well as analyzing the intramolecular interactions of the polymer in the absence of drug. Such analysis is based on the radius of gyration, solvent accessible surface area, and radial distribution functions.

METHODOLOGY

Materials. The model compounds used in this study were purchased from Euroasia Chemicals (Euroasia Ltd., China), Attix Pharmaceuticals (Toronto, Ontario, Canada), Chempacific

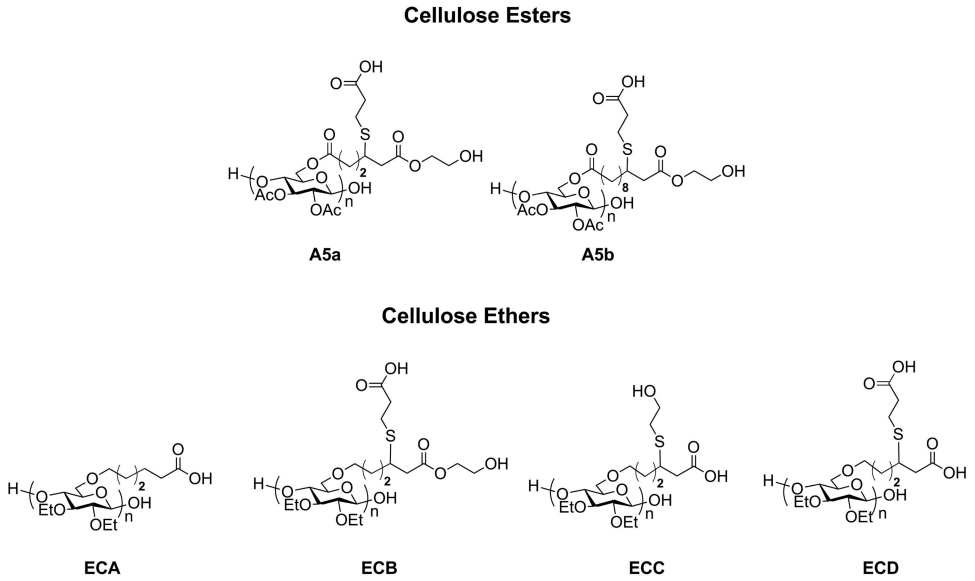

Figure 1. Molecular structures of synthesized cellulose polymers. Note that structures are not meant to imply regiospecificity; particular positions of substitution in all schemes are only for convenience of depiction and clarity.

DOI: 10.1021/acs.biomac.8b01280
Biomacromolecules 2018, 19, 4593−4606

Table 1. Polymer Abbreviations and Degree of Substitution for Newly Synthesized Cellulose-Based Polymers

#	polymer abbreviation	equivalent abbreviation	substituent 1 (DS)	substituent 2 (DS)	substituent 3 (DS)
1	CA-A5a-079	CA-Pen079-HEA-3MPA	acetyl (1.82)	A5a (0.79)	OH (0.39)
2	CA-A5b-067	CA-Un067-HEA-3MPA	acetyl (1.82)	A5a (0.67)	OH (0.51)
3	ECA-0.69	EC2.30C5-AA-H	ethyl (2.3)	ECA (0.69)	OH (0.01)
4	ECB-0.69	EC2.30C5-HEA-3MPA	ethyl (2.3)	ECB (0.69)	OH (0.01)
5	ECC-0.69	EC2.30C5-MA-2ME-TBAOH	ethyl (2.3)	ECC (0.69)	OH (0.01)
6	ECD-0.69	EC2.30C5-BA-3MPA-TBAOH	ethyl (2.3)	ECD (0.69)	OH (0.01)

(Baltimore, MD), ChemShuttle (Union City, CA), and Hawkins (Minneapolis, MN). Table S1 describes the supplier for each compound shown in Figure 2. The new cellulose-based polymers were synthesized as described in the next subsection. The aqueous medium used in all experiments was 100 mM sodium phosphate buffer pH 6.8, prepared by adding 6.96 g sodium phosphate dibasic anhydrous and 7.04 g monosodium phosphate monohydrate, made up to 1 L with deionized water.

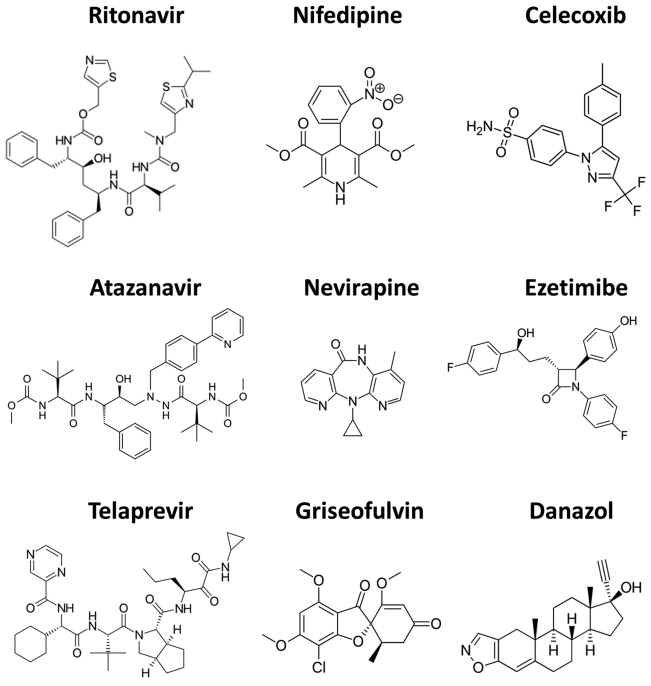

Figure 2. Chemical structures of model compounds.

Polymer Synthesis. The ω-carboxy cellulose ester/ether derivatives used in this study were prepared through a previously reported olefin cross-metathesis (CM) pathway, and are fully described including degree of substitution (DS) values in Table 1.[32−35] The mild nature of CM (37 °C, 2−3 h) permits attachment of a wide variety of functional groups (including carboxyl and different esters), and subsequent hydrogenation eliminates the tendency to cross-link, which would lead to loss of solubility of α,β-unsaturated CM products.[13,36] Furthermore, instead of hydrogenation, a tandem CM/thiol-Michael addition also removes α,β-unsaturation, while affording branched structures and additional functionality through the thioether.[14,32]

All polymers were made from olefin-terminated cellulose ester/ether derivatives, whose olefin substituents served as metathesis "handles" for functionalization with different CM partners. Polymers CA-A5a-079 and CA-A5b-067 were made from a commercial cellulose ester, cellulose acetate (DS 1.8, CA-320S), through esterification with undec-10-enoyl chloride[32,35] and pent-4-enoyl chloride,[32,36] respectively. Polymers ECA-0.69, ECB-0.69, ECC-0.69, and ECD-0.69 were made from microcrystalline cellulose through a one-pot etherification with ethyl iodide and 5-bromo-pent-1-ene.[13,14] Polymer syntheses for this study can be categorized into three reaction pathways:

Reaction pathway 1: 5-Carboxypentyl derivative ECA-0.69 was prepared by CM of EC2.30C5 with acrylic acid followed by hydrogenation to eliminate the α,β-unsaturation and provide a stable product.

Reaction pathway 2: Branched polymers CA-A5a-079, CA CA-A5b-067, and ECB-0.69 were synthesized by CM with hydroxyethyl acrylate followed by a thiol-Michael addition with 3-mercaptopropionic acid.

Reaction pathway 3: ECC-0.69, and ECD-0.69 were made by CM with methyl acrylate or benzyl acrylate, thiol-Michael addition with either 2-mercaptoethanol or 3-mercaptopropionic acid; and a further saponification using tetrabutylammonium hydroxide to remove the ester and recover an additional carboxyl group.[14]

Nucleation Induction Times. Polymers were predissolved in a small amount of DMSO and sonicated for 90 min at 50 °C until fully dissolved. Next, small aliquots of the DMSO solution were added, using constant agitation, to 20 mL of pH 6.8 100 mM buffer at 50 °C. After complete dissolution, the solutions were equilibrated at room temperature, and the volume was adjusted to obtain 5 μg/mL polymer solutions. The final solution had less than 1% DMSO. The methodology has been described by Dong et al.[14]

Supersaturated solutions were created by adding a specific amount of the drug stock solution to 47 mL of phosphate buffer, maintained at 37 °C and magnetically stirred at 300 rpm. The crystallization induction time from unseeded samples was measured using an SI Photonics UV/vis spectrometer (Tucson, AZ) coupled to a fiber optic probe (path length 0.5 or 1 cm). Measurements at two different wavelengths were recorded every minute. The time at which simultaneous increase in absorbance at the nonabsorbing wavelength and decrease at the absorbing wavelength were observed was taken as the induction time.

Telaprevir concentration was above its glass−liquid phase separation (GLPS) concentration; concentrations for the other eight drugs were below the LLPS or GLPS concentration of each. Details about the experimental conditions used in the nucleation induction time experiments are shown in Table S1. Table S2 describes the crystalline and amorphous solubility values of the compounds studied; the values have been previously determined in our group.

Atomic Force Microscopy (AFM). A MultiMode 8 AFM (Bruker Nano Surfaces, Santa Barbara, CA) was employed to characterize polymer interaction with amorphous surfaces. Samples were prepared by melting atazanavir onto stainless steel AFM pucks, which were then flattened using glass coverslips, and allowing it to cool, leaving nominally flat and

DOI: 10.1021/acs.biomac.8b01280
Biomacromolecules 2018, 19, 4593−4606

smooth amorphous surfaces. AFM was conducted in buffer solutions containing 5 μg/mL polymer. Characterization was performed in tapping mode, utilizing NPG-10 (cantilever C, 0.24 N/m spring constant, 30 nm nominal tip radius) silicon nitride triangular probes (Bruker Nano Surfaces, Santa Barbara, CA).

Both height and phase contrast images were obtained for each sample. Height plots provide topographical information on surfaces by measuring cantilever tip deflection and relating this data to the *z*-position of the surface. Phase contrast plots depict changes in cantilever resonance caused by interactions with the surface. Such interactions are sensitive to material properties of the surface, hence allowing for discrimination between polymer species and the underlying amorphous surface. Images were analyzed using NanoScope Analysis (v 1.5, Bruker Nano Surfaces, Santa Barbara, CA).

Computational Simulations. Fully atomistic classical MD simulations were performed to provide insight into the intra- and intermolecular interactions between polymer and drug molecules. Simulated systems included (1) a 28-monomer polymer chain in water, (2) a 25-molecule drug aggregate in water, and (3) the polymer chain (1) in the presence of the drug aggregate (2) in water. Six different polymers (Figure 1) were used, and telaprevir (TPV) and atazanavir (ATZ) were the model drug compounds. Importantly, the total number of molecules (187457) was maintained constant for all simulations performed.

MD simulations were carried out in GROMACS 5.0,[37,38] using the CHARMM force field.[39,40]

Construction of Polymer Chains. First, the structures of oligomers with four cellulose monomers were drawn in HyperChem 8.0.3.[41] The substitution patterns are shown in Table 2

Table 2. Substitution Patterns for Cellulose Ester Derivatives, where C_2, C_3 and C_6 Represent the Positions in a Cellulose Ring

carbon	monomer 1	monomer 2	monomer 3	monomer 4
C_2	Ac	Ac	Ac	H
C_3	Ac	Ac	H	H
C_6	A5x group	Ac	A5x group	Ac

Table 3. Substitution Patterns for Cellulose Ether Derivatives

carbon	monomer 1	monomer 2	monomer 3	monomer 4
C_2	Et	Et	Et	Et
C_3	Et	Et	Et	H
C_6	ECx group	Et	ECx group	Et

and 3, where acetyl (Ac), ethyl (Et), A5x (meaning A5a or A5b), and ECx (where x signifies A, B, C, or D) represent the functional groups shown in Figure 1. The substitution patterns of Tables 2 and 3 are chosen to resemble the probable locations and average quantities of the different substituents described in Table 1. This substitution pattern is also illustrated in Figure 3.

Second, an energy minimization of the oligomers with four monomers was performed with the Polak-Ribière (conjugate-gradient) algorithm, employing the BIO+(CHARMM) force field in HyperChem, using a maximum of 3×10^5 steps, and a root-mean-square (RMS) gradient of 1.0×10^{-2} kcal Å^{-1} mol^{-1} as the convergence condition. The structures were then submitted to the online topology building tool SwissParam,[42] used to obtain topology files in GROMACS format.

Using the included topology file provided by SwissParam, a residue topology file was constructed by using the GROMACS Topology Tools program by Anton Feenstra. This residue topology file was edited to create initial-, middle-, and end-type residues, where each residue (or oligomer) was composed of 4 monomers. Bonded and nonbonded parameters are taken directly from the CHARMM force field. Atomic charges were fitted to reproduce the electrostatic potential of a Hartree–Fock wave function mapped on a grid surrounding the oligomer to be parametrized. The ChElPG method was employed for this purpose. Partial charges on symmetrically equivalent atoms, for example, hydrogens on a methyl group, were balanced to avoid chiral effects.

Next, a polymer chain composed of 28 monomers (seven repeating units of four monomers each) was drawn in HyperChem 8.0.3 and minimized using the same conditions described in the previous step.[41] Notice that the total number of carboxylate groups in a 28 monomer system is 14 for A5a, A5b, ECA, ECB and ECC, while it is 28 for ECD.

MD Simulations of Single Chains. The polymers were solvated using the extended simple point charge (SPCE) water model. A total of 14 Na^+ ions were used as mobile counterions for the A5a, A5b, ECA, ECB, and ECC polymers, while 28 Na^+ ions were used for the ECD polymers. These ions served as counterions to the carboxylate groups of the polymer. The largest chain had 1298 atoms. The system included ∼187400 water molecules (varying depending on the absence or presence of drug molecules) in cubic boxes with edges of up to 17.9 nm.

Two equilibration stages and a production run were performed in GROMACS 5.0. The velocity-Verlet algorithm was used as integrator. Periodic boundary conditions were employed with the Verlet cutoff scheme for neighbor searching. Short-range electrostatic interactions were modeled with a cutoff of 1 nm, and the Particle Mesh Ewald (PME)[43] method was used for long-range electrostatics. van der Waals forces were calculated until a cutoff of 1 nm. Different energy groups, corresponding to drug, polymer, solvent, and ions, are specified in the MD simulation parameter files.

First, the system was minimized using the steepest descent algorithm (0.01 fs/step), and the minimization was stopped when the maximum force was less than 100.0 kJ mol^{-1} nm^{-1}.

Second, a canonical ensemble equilibration (NVT) was performed for 5 ns (1 fs/step) using the v-rescale thermostat, at a reference temperature of 310 K, with a coupling constant (tau-t) of 0.2 ps.

Third, a fast isothermal–isobaric equilibration (NPT) was employed for 1 ns (1 fs/step) using the v-rescale thermostat, at a reference temperature of 310 K, with a coupling constant (tau-t) of 0.2 ps; and the Berendsen barostat at a reference pressure of 1 bar, with a coupling constant (tau-p) of 0.2 ps.

Finally, the production run was performed for 5 ns (1 fs/step recording output every 2 ps) in the isothermal–isobaric (NPT) ensemble using the Nosé–Hoover thermostat, at a reference temperature of 310 K, with coupling constant (tau-t) of 0.2 ps, and the Martyna-Tuckerman-Tobias-Klein (MTTK) barostat at a reference pressure of 1 bar, with coupling constant (tau-p) of 1.0 ps.

The trajectories from the production run were examined. The radius of gyration (R_g), radial distribution functions (RDF), solvent accessible surface (SAS) areas, and an estimate of the free energy of solvation were analyzed for each type of oligomer. Details about computing R_g and SAS can be found in our

DOI: 10.1021/acs.biomac.8b01280
Biomacromolecules 2018, 19, 4593–4606

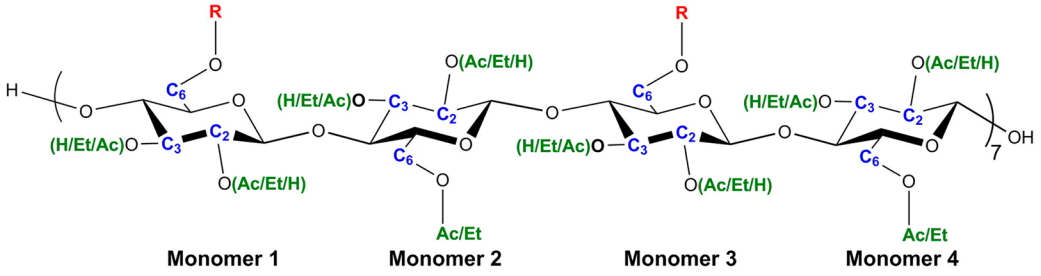

Figure 3. Oligomer of four cellulose monomers, as described in Tables 2 and 3. The green groups are either acetate, ethyl, or hydrogens, depending on the polymer type; and the R group in red has either one carboxylic acid (A5a, A5b, ECA, ECB, and ECC) or two carboxylic acids (ECD).

previous article.[7] The free energy of solvation of the polymer chains was estimated using a semianalytical algorithm implemented in GROMACS, called by adding the -odg option to the gmx sasa command.[44] This technique allows for estimation of average solvation free energies from per-atom solvation energies derived from exposed surface area along the trajectory. Those surface areas are computed using the double cubic lattice method by Frank Eisenhaber.[45]

MD Simulation in the Gas Phase to Create Drug Aggregates. The starting chemical structures of telaprevir and atazanavir were extracted from a crystalline structure report.[46,47] The sulfate molecules were removed from the structure reported for atazanavir bisulfate, because we were interested in the atazanavir free base. Using the Q-Chem 4.3[48] computational chemistry package, the structures were optimized using tight convergence criteria for the self-consistent field procedure. Density Functional Theory (DFT) calculations, with the hybrid Perdew–Burke–Ernzerhof exchange-correlation density functional (PBE0)[49,50] with Pople's 6-31+G* basis set were performed. The drug structures were then submitted to the online topology building tool SwissParam,[42] used to obtain topology files in GROMACS format.

A total of 25 drug molecules were added to a cubic box with edges of up to 6.0 nm. The system with atazanavir drug molecules underwent a 2 ns NVT equilibration, followed by 6 ns NPT equilibration, and the system with telaprevir drug molecules underwent a 0.5 ns NVT equilibration, followed by 2 ns NPT equilibration. The sole purpose of these simulations was to create aggregates of drug molecules in the gas phase. For the NVT equilibration the v-rescale thermostat, at a reference temperature of 310 K, with a coupling constant (tau-t) of 0.2 ps was used. For the NPT equilibration, a coupling constant (tau-t) of 0.2 ps and the MTTK barostat at a reference pressure of 1 bar, with coupling constant (tau-p) of 1.0 ps, were utilized.

Polymer–Drug MD Simulations. The aggregate of 25 drug molecules was placed in the presence of a polymer chain previously equilibrated as described above. Then the water solvation box was adjusted to fit both solutes. The simulations were performed starting with the drug aggregate and the polymer separated by a short distance of approximately 1 to 2 nm. A NVT equilibration stage was performed (0.5 ns), followed by a NPT equilibration (1 ns) using the v-rescale thermostat and the Berendsen barostat, a second NPT equilibration (5 ns) using the Nosé–Hoover thermostat and the MTTK barostat, and a NPT production run (10 ns) using the Nosé–Hoover thermostat and the MTTK barostat.

For the polymer–drug interaction analysis, the Lennard-Jones and Coulomb terms for short and 1–4 interactions were extracted. The GROMACS energy function was run for all energy groups, with the flag "-fee" to estimate the free energy difference with respect to an ideal gas state along the production trajectory.[51] Equation 1 shows the description of the free energy estimate, where k is the Boltzmann constant, T is the simulation temperature, 310 K, U is the potential energy of the polymer–drug interaction. In the case of the polymer–drug interaction, the free energy estimate is obtained by employing a regular free energy perturbation approach, as an average computed between all recorded steps of the trajectory.

$$\Delta G = G_{(n,P,T)} - G_{\text{ideal gas}(n,P,T)} = kT \ln\langle e^{U/kT}\rangle \quad (1)$$

RESULTS

Nucleation Induction Time. The crystallization inhibition properties of cellulose-based polymers were evaluated. The model drugs used for the studies included fast, intermediate, and slow crystallizers. Griseofulvin, celecoxib, ezetimibe, and danazol were fast crystallizers; telaprevir, nifedipine, and nevirapine were intermediate; and ritonavir and atazanavir were slow crystallizers. The drugs were un-ionized at the pH values used in these experiments, pH 6.8; hence, ionic interactions between drug and polymer were absent.

The polymer concentration in these experiments was 5 μg/mL. The viscosity of the buffer solution remains unchanged at these low concentration values. Furthermore, the synthesis method used (cross-metathesis and thiol-Michael addition) was mild and modular.[14,32,52] Thus, similar molecular weight distribution is expected (more information is provided in Supporting Information). Consequently, the variations in nucleation induction times cannot be attributed to changes in the viscosity of the solutions or the polymer molecular weight, but to the different substitution patterns.

All polysaccharide derivatives studied had carboxylic acids. The DS(CO_2H) was kept constant for each derivative type, and the DS of carboxyl-bearing substituent was held within a narrow range (0.67–0.79) across the range of polymers studied (Figure 1; but note that one polymer type, ECD, bears two carboxyls per substituent). The main differences between the cellulose ethers and cellulose esters were the linkage to the cellulose backbone, and the nature of the starting material used to synthesize the polymers. Cellulose acetate was modified to make the cellulose esters used in this study, while ethyl cellulose was used to make the cellulose ethers.

Figure 4 shows the effectiveness of two cellulose esters that differ only in the length of the hydrocarbon tether that attaches the functional group (e.g., carboxyl) to the cellulose backbone. Polymer CA-A5a-079 has a short tether, while polymer CA A5b-067 has a long tether (Figure 1). The polymer with the

DOI: 10.1021/acs.biomac.8b01280
Biomacromolecules 2018, 19, 4593–4606

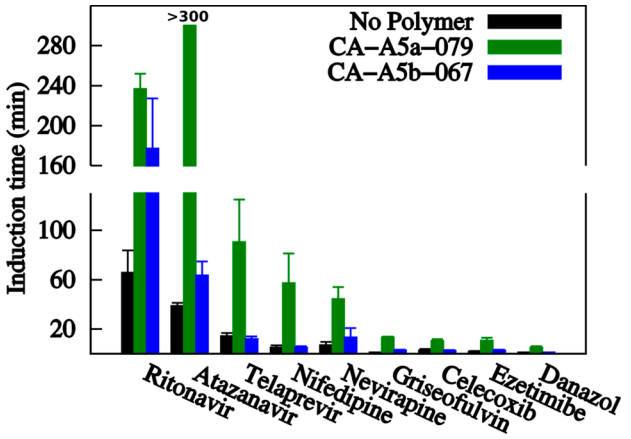

Figure 4. Induction time for nine drugs in pure buffer (black bars) or in buffer containing 5 μg/mL of a cellulose ester polymer (green and blue bars; number of experiments, n = 3).

short tether performs better than the polymer with the long one for all the compounds studied.

Consequently, the next set of polymers were designed with a short hydrocarbon tether. Cellulose ethers were designed with variations in the position of the carboxylic acid group, as shown in Figure 1. Figure 5 shows the nucleation induction times for

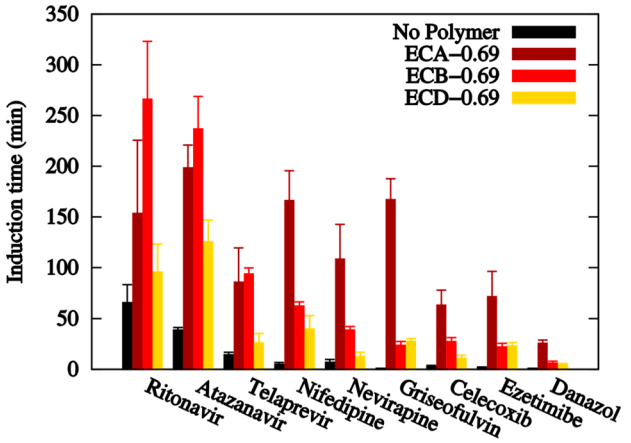

Figure 5. Induction time for nine drugs in buffer (black bars) or in buffer containing 5 μg/mL of a cellulose ether polymer (red and gold bars; n = 3).

the same group of drugs, in the presence of differently designed cellulose ether derivatives: one with a single chain ending with a carboxylic acid (ECA-069) per CM substituent, one with a two branches, one with a terminal carboxylic acid and one with an alcohol (ECB-069), and one with two branches each of which terminates with a carboxylic acid (ECD-069). ECA-0.69 appears to be an effective crystallization inhibitor, especially for the fast crystallizing compounds. For slowly crystallizing compounds, those with longer induction times, the polymer with a single terminal carboxylic acid (ECB-069) is more effective than the polymer with two terminal carboxylic acids (ECD-069), while little difference is apparent between the two polymers for the fast crystallizing compounds.

Adsorption of the Polymer onto Atazanavir Amorphous Films. Atomic force microscopy (AFM) was used to study how the polymer adsorption varies on amorphous films of drug. Changes in topographical and phase contrast AFM images give an indication about the tendency of the polymer to interact with the amorphous surface, which is indirectly related to intra- and intermolecular interactions between drug, polymer, and water.[53] Figure 6 shows variations in phase and height for amorphous films of atazanavir exposed to different polymer solutions. Globular structures are observed in the presence of A5b, ECA, ECB, and ECD, whereas they are absent in the presence of A5a.

The height figures allow for direct quantitation of polymer globule dimensions. Phase contrast plots aid in interpretation of features in the height plot, assisting in discrimination between adsorbed polymers and topographical features on the underlying surface. Additionally, phase plots provide enhanced contrast relative to height plots for interrogation of finer structural features. For example, the phase plot for the ECD system reveals some smaller globules that are hidden within the surface topography on the height plot. Furthermore, some larger globules on the height plots for ECB and ECD can be distinguished on the phase plot as agglomeration of multiple smaller globules.

MD Simulations. First, MD simulations of single polymer chains were performed to determine whether variations in the chemical structure of the polymer translate into changes in the dynamic behavior of the chain. The radius of gyration, solvent accessible surface area, estimated free energy of solvation, and radial distribution functions were computed. These simulations were performed with single chains to simplify the system and avoid interference by other components. The polymer chains were drawn to resemble the average location of the different substituents. Nonetheless, the real polymers are randomly substituted and, as a result, may slightly differ from the model system either in DS or in substituent locations.

Figure 7a shows the free energy of solvation, estimated from the MD production trajectory. This indicates that the cellulose ester polymers (A5a and A5b) have more negative free energies of solvation than the cellulose ether polymers based on ethyl cellulose (ECA, ECB, ECC, and ECD). Figure 7b shows the solubility parameters calculated by the Fedors method for comparison purposes, where more positive values indicate more hydrophilic materials.[54] Importantly, the MD simulations correspond to the ionized state of the polymers, which is expected under the experimental conditions employed, while the solubility parameter calculations correspond to neutral structures, because the Fedors method forbids the inclusion of ionized substituents.

The results from Figure 7a,b indicate that the process of solvation of the A5a and A5b polymers is more favorable than for the EC polymers. When comparing A5a and A5b, which only differ in the hydrocarbon tether length, it is more favorable to solvate A5a (short tether) than A5b (long tether), as expected. Furthermore, drastic differences are observed in the estimated free energy of solvation and in the solubility parameter when comparing A5a and ECB. These two polymers possess similar side chain length and functional group (i.e., carboxylic acid) but differ in the linkage to the cellulose backbone (ester versus ether), the additional substituent, and the DS (acetyl versus ethyl, Figure 1 and Table 1). This suggests that, although chemical structures may look similar, small variations in the chemical structure and DS may influence the solvation process.

Figure 7a shows that among the EC derivatives, ECC has the most positive estimated free energy of solvation, indicating that it may be harder to solubilize. This is an interesting observation because the solubilization process for the ECC polymer

DOI: 10.1021/acs.biomac.8b01280
Biomacromolecules 2018, 19, 4593−4606

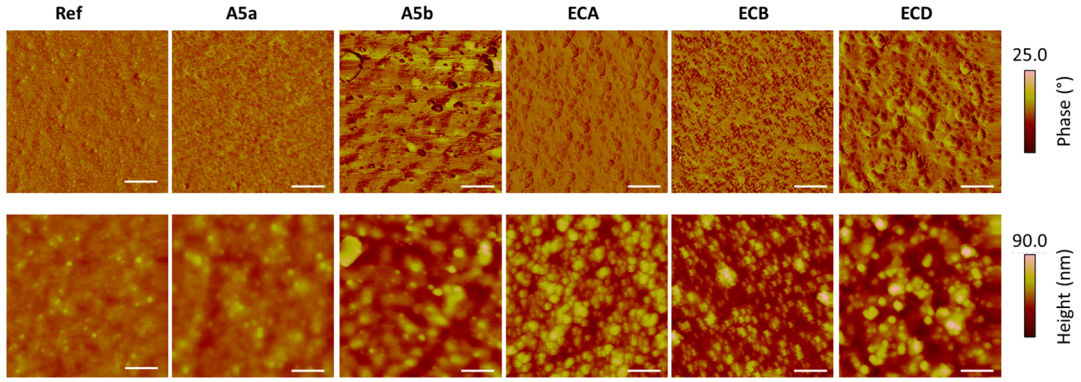

Figure 6. AFM height (2 μm × 2 μm) and corresponding phase contrast images for atazanavir in the absence (ref) and presence of polymers (A5a, A5b, ECA, ECB, and ECD). Images were captured in liquid at room temperature and with a 1 h incubation period. Scale bars represent 400 nm.

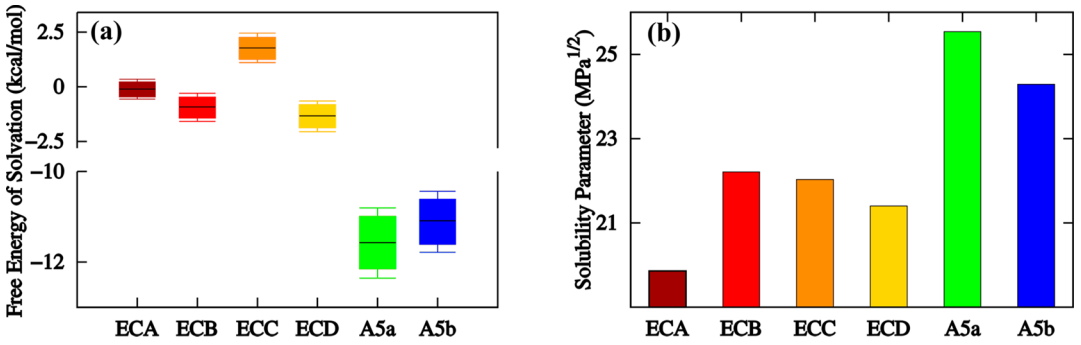

Figure 7. (a) Free energy of solvation for a group of seven oligomers with 28 monomeric units. Data processed from the production trajectory. The arithmetic mean is marked by the black horizontal line, accompanied by candlesticks, centered on the median, representing the standard deviation. The whisker bars mark the lower and higher quartiles, meaning that 50% of all measurements are contained within these bars. (b) Solubility parameter calculated by the Fedors method.

was particularly challenging, due to precipitation upon contact of the DMSO−polymer solution with buffer. This complication is the reason that experimental results are not shown.

The radius of gyration, R_g (Figure 8a), and solvent accessible surface areas (SASA) per atom (Figure 8b) were analyzed for the production trajectory for single chain systems. We have previously used these quantities to analyze the structure of a wide range of cellulose ester polymers and have observed that the R_g primarily depends on the conformation of the main cellulose chain, while the SASA depends on the conformation of the side chains.[7] The R_g values (Figure 8a) for the 28-monomer chains are in the 2.9−3.7 nm range. Two main observations were made from these results: (1) the A5a cellulose chain is more extended than the A5b chain and (2) the ECC chain has a high distribution of R_g values during the trajectory indicating that this polymer structure is more flexible and that the cellulose chain tends to have a greater variety of conformations.

The SASA values (Figure 8b) show a higher area for the ECA, ECD, and A5a polymers, indicating that the side chains are more extended in these systems, and the lowest value is for A5b (long hydrocarbon chain), indicating that the side chains in A5b tend to be more agglomerated.

We then performed simulations of a polymer chain with a nucleus of 25 drug molecules. Experimentally, the polymer is first dissolved and equilibrated in an aqueous environment, followed by addition of the drug solution. Thus, for this set of simulations, the polymer structure chosen corresponded to the equilibrated state after performing simulations for lone-polymer chain systems. In other words, all the simulations with the lone-polymer chains were performed initially, followed by the simulations with both the drug and the polymer chain. For the drug-and-polymer simulations, a nucleus of drug molecules was first prepared in the gas phase and then solvated. The reason for using a drug aggregate was the occurrence of these type of structures during experiments, rather than single solvated drug molecules. A set of simulations was performed starting from a conformation with close separation between the polymer and the drug aggregate, approximately 1−2 nm apart. It is expected that during the simulation the molecules would get closer if the interaction is favorable or would separate if the interaction is unfavorable.

Figure 8b,c show the R_g and SAS for the polymer during the production trajectory corresponding to the simulations of a combined polymer−drug aggregate system. Noteworthy, in some cases, the polymer R_g tends to be smaller in drug-and-polymer simulations than in lone-chain simulations, which indicates that the presence of the nearby drug aggregate influences the structure of the main cellulose chain. Interestingly, the A5b polymer is more agglomerated in the presence of both ATZ or TPV, suggesting that the interaction of A5b with the drug aggregates is less attractive compared to the more favorable intramolecular interactions of A5b. The SASA results (Figure 8d) show a similar trend in the absence of drug, where A5a has a higher solvent accessible surface area per atom than A5b.

We analyzed the interaction between polymer and drug. The probability of finding the polymer chain at a given distance from the aggregate of drug molecules is shown in Figure 9, represented through the radial distribution function (RDF) between polymer and drug.

DOI: 10.1021/acs.biomac.8b01280
Biomacromolecules 2018, 19, 4593−4606

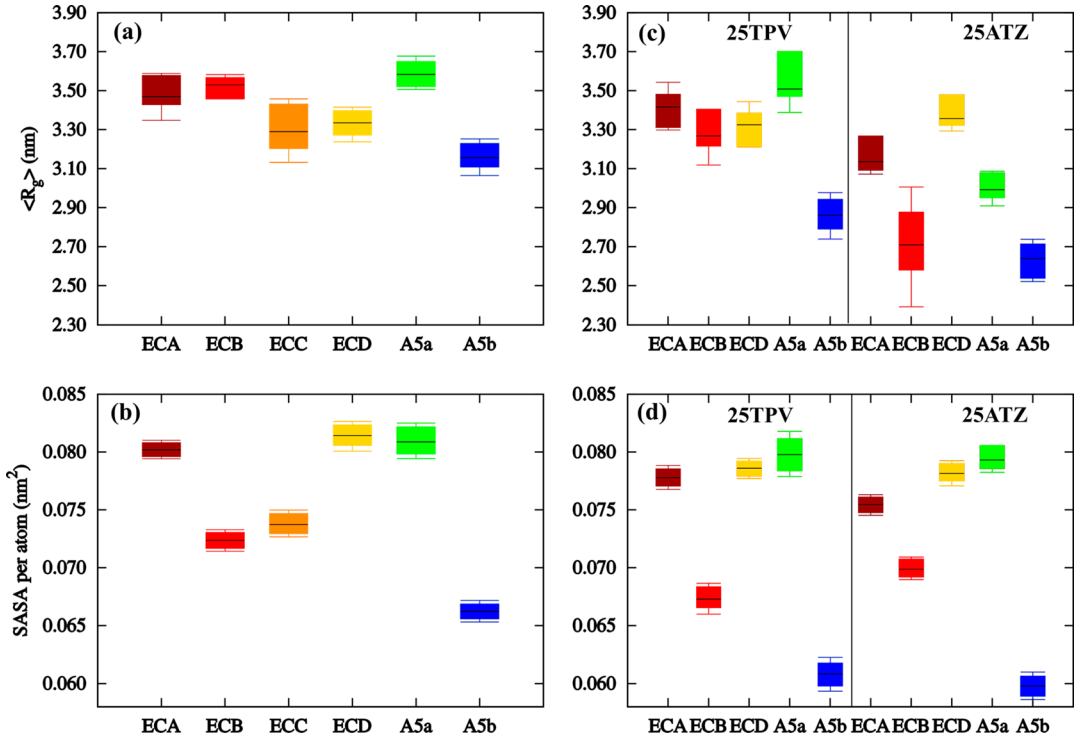

Figure 8. (a, c) Average radius of gyration $\langle R_g \rangle$ and (b, d) solvent accessible surface area per atom for a group of seven oligomers with 28 monomeric units. Data processed from the production trajectories. (a, b) Conformations from the single chain simulations. (c, d) conformations from the polymer–drug simulations. The arithmetic mean is marked by the black horizontal line, accompanied by candlesticks, centered on the median, representing the standard deviation. The whisker bars mark the lower and higher quartiles, meaning that 50% of all measurements are contained within these bars.

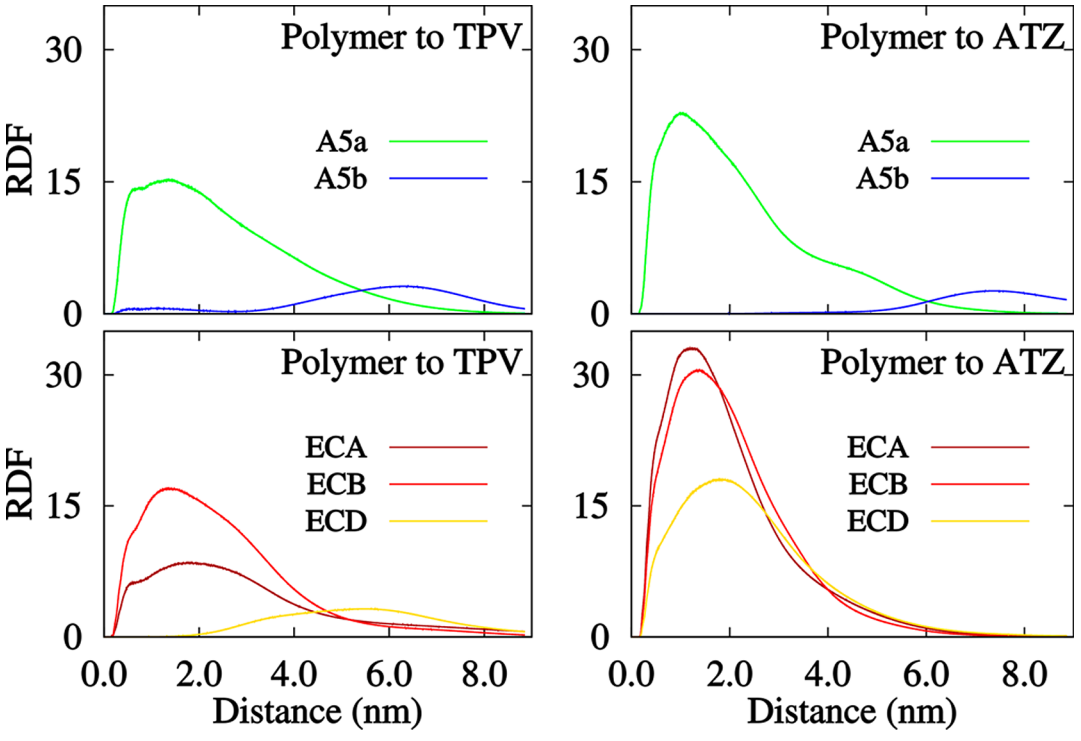

Figure 9. Radial distribution function (RDF) between polymer and drug molecules, corresponding to the 10 ns production trajectory.

Among the nine compounds studied experimentally, TPV and ATZ have been more extensively used to explore the effectiveness of newly synthesized cellulose polymers and crystallization inhibition in general.[7,55,56] Therefore, TPV and ATZ were selected as model drugs for the MD simulations. This selection could also prove useful in future studies as we continue optimizing and validating the computational methodology described herein and conducting additional studies on these representative poorly soluble compounds.

Comparison of ATZ and TPV in the presence of A5a, A5b, ECA, ECB, and ECD are shown. The results indicate that there is a higher probability of finding A5a closer to the drug

DOI: 10.1021/acs.biomac.8b01280
Biomacromolecules 2018, 19, 4593–4606

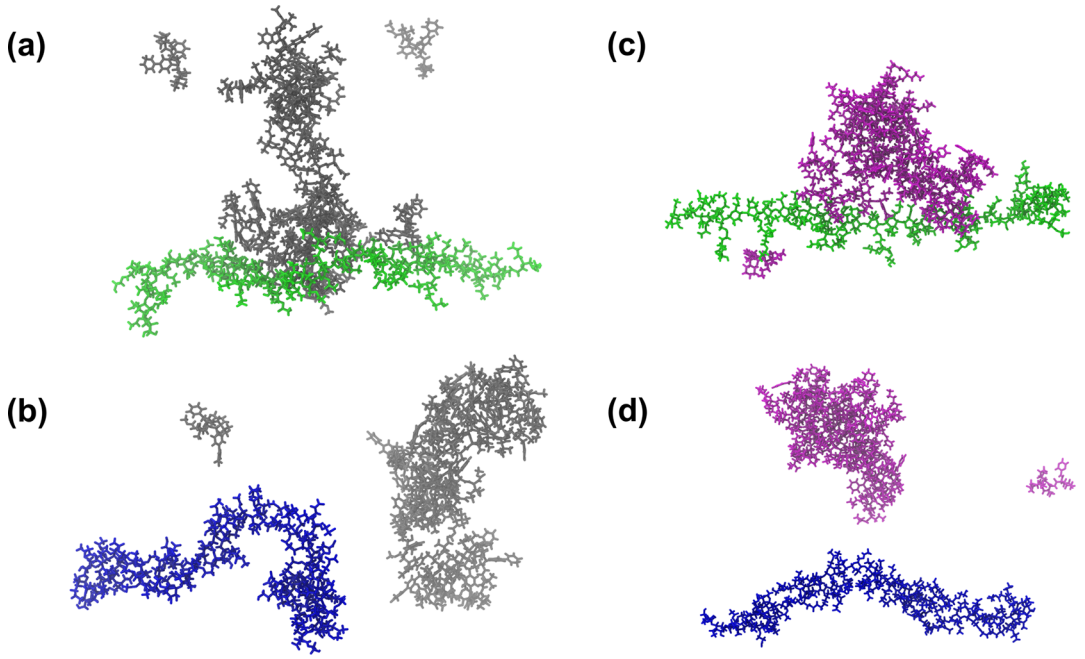

Figure 10. Representative snapshots from the 10 ns production trajectories. ATZ molecules are shown in gray, TPV molecules are magenta, A5a is green, and A5b is blue: (a) ATZ and A5a; (b) ATZ and A5b; (c) TPV and A5a; and (d) TPV and A5b.

molecules than A5b. Nonetheless, there is a greater attraction between A5a and ATZ than between A5a and TPV, represented by a higher RDF peak. Figure 10 shows illustrative snapshots from the production trajectories for the drug with A5a or A5b systems. Regarding the EC polymers, there is a higher probability of finding ECA and ECB close to the drug aggregate than ECD, especially for TPV.

Next, we determined the probability of finding certain sections of the polymer close to the drug aggregate. Specifically, we were interested in comparing the probability of finding the carboxylate group (COO^- termination) or the ethyl or acetyl group (CH_3 termination) close to the drug aggregate. Figure 11 shows the RDF for two of the most effective polymers (A5a and ECB) for TPV and ATZ, and one of the less effective polymers (ECD). Figure 11 indicates that there is a lower probability of finding the carboxylic acid group than the more hydrophobic group, CH_3, close to the drug aggregate for these systems.

Different energy groups were specified in the MD simulation parameters file to enable the extraction of information about the intermolecular interactions between drug and polymer. Figure 12 shows an estimate of the free energy difference with respect to the ideal gas state, which is calculated over the full 10 ns of the trajectory at 310 K. According to these results, the interaction of A5b with the nucleus of drug molecules is insignificant for both TPV and ATZ. Meanwhile, A5a interacts with ATZ and TPV, with a more negative value for ATZ, indicating a more attractive interaction between ATZ and A5a. ECA and ECB have an attractive interaction with TPV, but the interaction appears to be stronger between ECB and TPV than between ECA and TPV, and ECD interacts marginally with TPV. In contrast, ATZ has an attractive interaction with ECA, ECB, and ECD, but the interaction is stronger with ECA and ECB than with ECD.

DISCUSSION

The increasing interest in amorphous solid dispersion as a strategy to improve drug solubility, driven by the rising number of drugs with solubility issues, creates a need to find new materials that delay crystallization from these metastable formulations. It has been reported that several additives, such as polymers and bile salts, have crystallization inhibition properties, which makes them attractive excipients for drug formulations.[7,9,15,55−57] Herein, different cellulose-based polymers with carboxylic acid functionalities were synthesized to determine how variations in chemical structure influenced their performance at inhibiting drug crystallization. The polymers synthesized had carboxylic acid functionalities, based on our previous observations showing that polymers with carboxylic acids were more effective than those with amides, amines, or alcohols.[7] We had previously studied the effectiveness of A5a and A5b for TPV and found that the variation in the length of the hydrocarbon chain had a drastic impact on the effectiveness of the polymer, with A5a (short hydrocarbon tether) showing better effectiveness than A5b (long hydrocarbon tether).[7] These results suggested that the intramolecular interactions in the polymer significantly influenced their effectiveness at inhibiting crystallization: a polymer that tends to self-associate has a lower probability of interacting with drug molecules. However, one outstanding question was whether the same trend would be obtained for other drugs, with chemical properties different from TPV. This led to the exploration of the nucleation induction times for a group of nine drugs (Figure 2) in the presence of A5a and A5b. Interestingly, A5a performed better than A5b (Figure 4) for all the compounds studied, suggesting that the polymer ineffectiveness was probably due to its preferred self-interaction, which in turn leads to a low tendency to interact with the drug molecules.

A better understanding of what may be happening in solution can be extracted from the simulations of 28-monomer single-chain polymers as well as from the simulations of drug aggregates at a close distance of one of these polymer chains. Figure 8 shows that A5a has a more extended conformation than A5b, as evidenced from the R_g and SASA. It is also apparent that the presence of the drug, TPV or ATZ, has an impact on the polymer's intramolecular interactions. Particularly, A5b

DOI: 10.1021/acs.biomac.8b01280
Biomacromolecules 2018, 19, 4593−4606

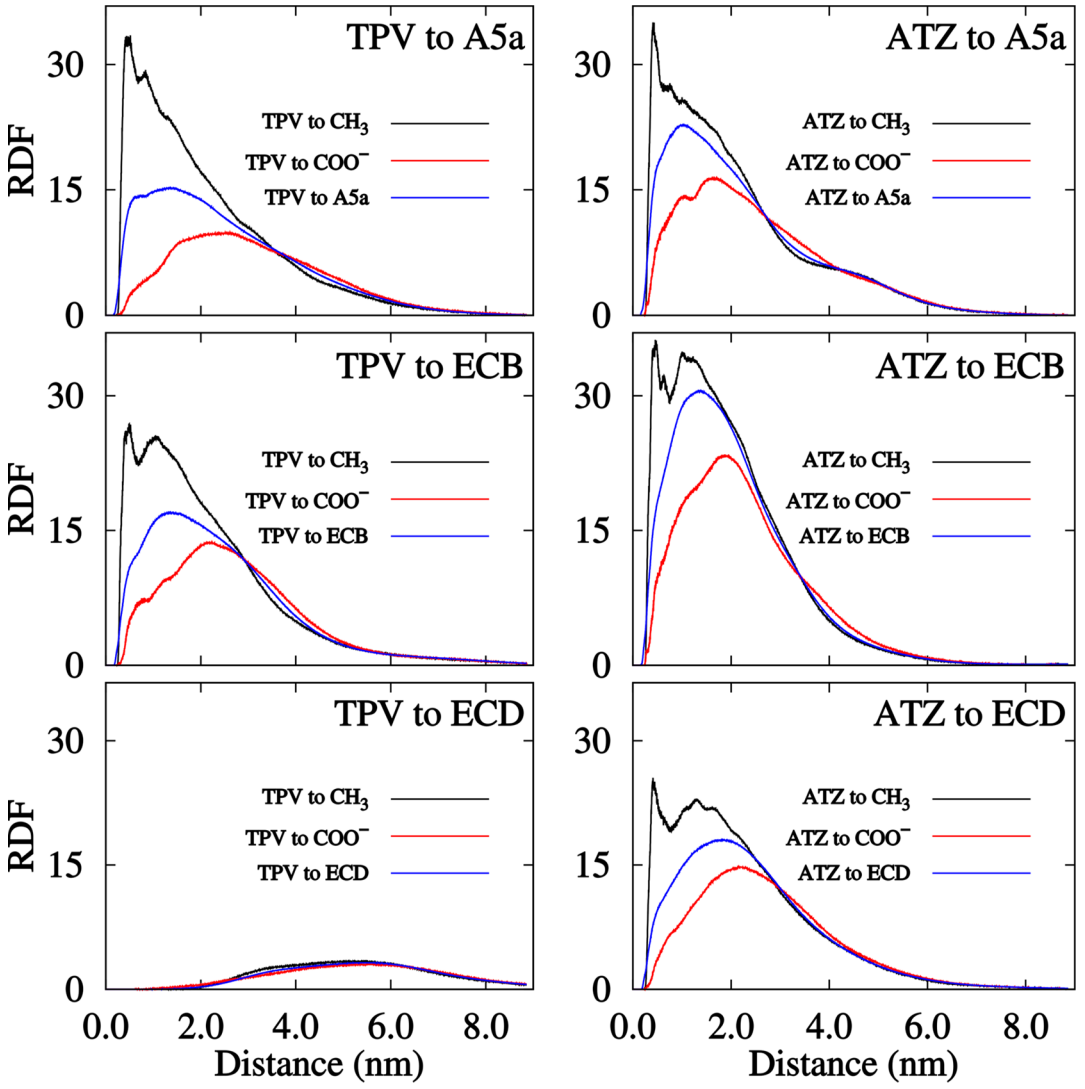

Figure 11. Radial distribution function (RDF) between polymer and drug molecules, corresponding to the 10 ns production trajectory. The black line denotes the RDF between the CH_3 group in the acetyl or ethyl group and the drug molecules; the red line denotes the RDF between the COO^- and the drug molecules; and the blue line denotes the RDF between all the atoms of the polymer and the drug molecules.

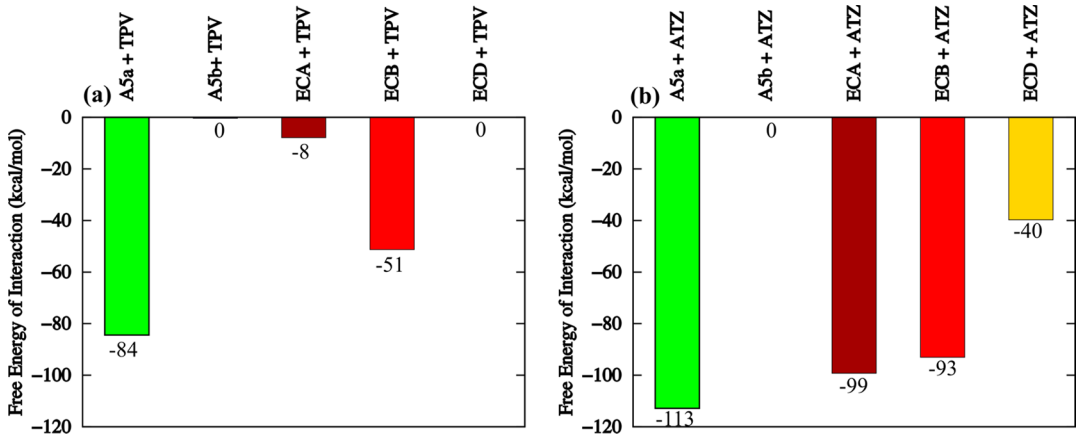

Figure 12. Estimated free energy of interaction for different polymer−drug systems, corresponding to the 10 ns production trajectory, and computed with respect to the ideal gas state, as described in eq 1.

tends to self-associate even more in the presence of ATZ and TPV, indicating that the self-interaction is favored instead of the drug-polymer interaction. The RDF results shown in Figure 9 are in good agreement with these results, where the probability of finding A5a close to the drug is much higher than the probability of finding A5b.

DOI: 10.1021/acs.biomac.8b01280
Biomacromolecules 2018, 19, 4593−4606

Given that A5a effectively extended nucleation induction times, new polymer candidates were created with similar structures but with an ether linkage to the cellulose backbone, and with ethyl cellulose as the starting material. The cellulose ether polymers have some potential advantages including hydrolytic stability under extreme pH conditions, and a potentially shorter synthetic route.

Cellulose ethers ECA, ECB, ECC, and ECD were of interest to illuminate how variations in the position and number of carboxylic acids per anhydroglucose unit (AGU) influenced their effectiveness. Unfortunately, ECC could not be used due to issues with polymer solubilization in an aqueous solvent. The aqueous solubility for the remaining ethyl cellulose derivatives (ECA, ECB, and ECD) is in the 1−11 mg/mL range.[58] ECA included a single single tether chain with a carboxylic acid termination, which permitted us to evaluate polymer effectiveness in the absence of additional branches. ECA was an effective crystallization inhibitor for all the compounds studied, but it was particularly effective for the fast crystallizing compounds, increasing the nucleation times by more than an order of magnitude in some instances. According to the R_g and SASA values in the absence of drug (Figure 8a,b), ECA adopts a conformation in which the main cellulose chain and the side chains are extended. This probably contributes to its favorable interaction with different types of drug molecules. The RDF values in Figure 9 support favorable interaction of ECA with drug molecules, showing a higher probability of finding ECA close to ATZ and TPV aggregates, with higher peaks in the case of ATZ.

ECB presents a structure similar to that of A5a, while ECD has two branches with carboxylic acids. Figure 5 shows that the presence of more carboxylic acid groups per AGU (ECD) may not improve polymer effectiveness as a crystallization inhibitor. The polymer with one carboxylic acid (ECB) performed better than the polymer with two carboxylic acids for most drugs; except for griseofulvin and ezetimibe, where both polymers appeared equally effective. This observation initially surprised us, considering that we have observed that carboxylic acid substituents typically lead to more effective polymers. Further, in previous studies, it appeared that polymers with higher DS (COOH) were better inhibitors, although those polymers had other structural variations in addition to DS (COOH).[8]

MD simulations for these systems allowed us to gain insight into differences between the ECB and ECD polymers at the molecular level and to decipher the reason behind the better effectiveness of ECB compared to ECD. The solvent accessible surface area measurements in the absence or presence of drug (TPV and ATZ) are larger for ECD than for ECB (Figure 8b,d), indicating that the side chains are more extended for ECD, with its two negative charges per AGU. It is important to point out that, two charges per AGU were simulated for the ECD polymer, but it is possible that under the experimental conditions used some of the carboxylic acid groups are protonated while others are ionized, since they influence one another's kinetics and extent of ionization.

The R_g of ECB and ECD was similar in the absence of the drug aggregate (Figure 8a), and it indicates an extended conformation of the main cellulose chain. Moreover, some variations are observed when the polymer is placed in the presence of the drug aggregate (Figure 8c). For instance, the R_g for ECB is reduced when it is in the presence of ATZ. Variations in the R_g of the polymer due to the presence of the drug aggregate can be explained in two ways. One is that the polymer has more attractive interactions with itself. Another is that the polymer is actively interacting with the drug aggregate, which results in the bending of the chain.

Therefore, an additional metric was required to determine the potential interaction between polymer and drug. RDF values (Figure 9) show a higher probability of finding drug molecules (TPV or ATZ) closer to ECB than to ECD, indicating a more attractive interaction between ECB and the drug, than between ECD and the drug. Consequently, the reduced R_g for ECB in the presence of ATZ can be attributed to a strong interaction with the drug aggregate, which results in bending of the chain. Overall, these MD results shed light into how the polymer with two carboxylic acids (ECD) had a lower probability of interacting with the drug aggregate than the polymer with one carboxylic acid (ECB), suggesting that by adding a second carboxylic acid group (ECD) we are actually weakening the polymer−drug interaction.

In addition, the RDF values between sections of the polymer and the drug aggregate (Figure 11) indicate that the interaction of the most effective polymers (A5a and ECB) with the drug molecules (TPV and ATZ) is mainly driven by the hydrophobic interactions between the acetyl/ethyl group and the drug aggregate, rather than specific interactions with the carboxylic acid group. The use of experimentally determined RDFs to study solid mixtures of ASDs,[59] as well as the interaction energy for solid mixtures[17,60] has been described in the literature as an alternative to study intra- and intermolecular interactions between drug molecules and polymer in the solid state. The results shown herein support the utility of this approach for understanding solution behavior.

The AFM measurements provide insight about the interaction of the polymer at the drug-water interface, precisely by providing visualization of how the polymer adsorbs to the surface of the amorphous drug. It is hypothesized that differences in the affinity of the polysaccharide derivative polymer for water versus drug will influence the conformation of the polymer adsorbed to the amorphous surface. Previous studies of polymers adsorbed to crystalline surfaces demonstrated a relationship between the extent of polymer coverage on the surface and the rate of crystal growth.[53] The current study uses an amorphous surface which provides a better representation of the initial disordered phase, thought to be the first stage of the nucleation process.[61]

Clear differences are seen between short and long hydrocarbon tether length cellulose esters when comparing their disposition on the surface of the atazanavir film (Figure 6). The polymer with the short tether appears to be homogeneously dispersed across the surface (A5a), while unevenly distributed large polymer globules are observed for the polymer with the long tether (A5b). These observations agree with the MD simulations, which show the tendency of the latter polymer to self-associate. Smaller globular structures are observed for ECA, ECB, and ECD. ECA and ECB structures have similar sizes and are uniformly spread throughout the surface, while larger globular structures are observed for ECD. Figure 5 indicates that ECA, ECB, and ECD inhibit crystallization for ATZ, with better performance exhibited by ECA and ECB. This suggests that even though these three polymers form globular structures, they are still able to inhibit crystallization. However, one of the main differences observed is in surface coverage by these globular structures, with more extensive coverage for ECA and ECB, less coverage by ECD, and even less by A5b. It is unsurprising that the EC polymers form these globular structures at the drug-water interface, as the MD simulations of

DOI: 10.1021/acs.biomac.8b01280
Biomacromolecules 2018, 19, 4593−4606

lone-polymer chains in water indicate that EC derivatives have more positive energies of solvation (Figure 7). The SASA is lower for ECB than A5a, indicating that the side chains are more contracted, and is approximately the same for ECA, ECD, and A5a (Figure 8b). The formation of globular structures onto the surface does not necessarily indicate that a polymer is a poor crystallization inhibitor. It is also necessary to determine polymer coverage of the surface and the size of the globular structures. It is possible that the formation of these globular structures may impact the ability of the polymer to prevent crystal growth, with better performance for polymers that are able to spread evenly and in an extended conformation, than for those that form globules with a low extent of surface coverage. Or it may be that a higher additive concentration is needed to inhibit crystallization for polymers which form globules.

We simulated drug aggregates in the presence of polymers to obtain a thermodynamic quantity, the free energy of interaction between drug and polymer, as a general indication of the likelihood of a polymer−drug interaction. The idea was inspired by protein + ligand simulations, which use thermodynamic cycles to compare the variations in the interaction energies when changing the chemical structure of the ligand.[1,20] These methodologies are widely used during discovery stages and are standardized for protein systems. There are multiple differences between proteins and polysaccharides that make simulations with polysaccharides systems more challenging. First, there are crystal structures available for proteins, which typically correspond to their quaternary structure; whereas polysaccharide structures are constructed from scratch. There is variability from polymer chain to polymer chain due to the random substitution patterns of these cellulose-based polymers, and their relatively broad distribution of degrees of polymerization. This implies an extra level of preparation for the simulations, where the structures are based on the percentages of substitution rather than in the actual position in the polymer chain. Second, proteins typically have pockets where the ligand will more likely interact, whereas drug molecules are expected to interact with different sections of the polysaccharide materials. Finally, polysaccharide derivatives are more flexible than proteins because they tend to lack ternary or quaternary structure. These factors make the simulation of polymer−drug systems more challenging for this type of calculations.

In the present study, we estimated the free energies of interaction (Figure 12) based on the 10 ns production trajectories. The results shown indicate that A5a interacts favorably with ATZ and TPV, while A5b does not come in close contact with the drug molecules. Similarly, ECA, and ECB have attractive interactions with ATZ and TPV, while ECD appears to interact more weakly, particularly with TPV. However, the interaction between ECA and ATZ is stronger than between TPV and ECA. These results agree with the experimental nucleation induction times shown in Figures 4 and 5, which suggest that the estimated free energy of interaction between drug and polymer may give valuable information about the tendency of the polymer to interact with the drug molecules and prevent crystallization. Interaction with the emerging nucleus is clearly a prerequisite for disruption of nucleation.[62] Therefore, polysaccharides that show little interaction clearly will be ineffective. However, for polymers with favorable interactions with the drug aggregate it is likely that the extent of nucleation disruption will also depend on the extent to which the drug self-association is disrupted by the presence of the polymer, whereby steric factors, such as bulkiness of side chain groups, may contribute.

It is important to highlight that crystallization depends on kinetic and thermodynamic factors. The MD simulations described herein only provide thermodynamic information. As a result, it is not realistic to expect a direct correlation between the induction time results and the estimated free energies of interaction. Rather, it is shown that the estimated free energies of interaction can give valuable information about the likelihood of a polymer interacting with a drug molecule.

Nevertheless, some of the limitations of the current methodology include the length of the simulated trajectory and the computational resources needed, even though the simulation times are in the nanoseconds range. The lack of an experimental structure for the polysaccharide (e.g., X-ray crystal structure) requires the extra step of creating the polymer chain and running simulations for lone polymer chains in water to obtain a structure that resembles the experimental.

For these reasons, careful planning is advised in the implementation of this type of methodology in an industrial setting, where fast results will be needed to serve as a screening methodology for polymers. Alternative methodologies, such as simulated annealing MD, may allow for a wider sampling of conformations. Different methods, such as semiempirical and tight-binding approaches, may provide useful static properties at a fraction of the current computational cost. Nonetheless, this study opens a promising extensive field to continue exploring.

CONCLUSION

This study involved a multifaceted experimental and theoretical approach to explain variations in the crystallization inhibition properties of a series of polysaccharide derivatives. Small changes in the chemical structure of the polymer strongly influenced its ability to inhibit crystallization. The determination of radial distribution functions and estimated free energies of interaction between a nucleus of drug molecules and a polymer chain, using computational modeling, were useful to predict possible intermolecular interactions in solution. The tendency of the polysaccharides to interact at the amorphous drug−water interface was verified by AFM measurements, whereby computational predictions showed good agreement with experimental data. These approaches lend support to the hypothesis that polysaccharides that are effective crystallization inhibitors have a balance of hydrophobic and hydrophilic groups. Thus, effective polysaccharides interact with drug aggregates via hydrophobic interactions with backbone functionalities such as ethyl groups, while carboxylate groups associated with tethered substituents lead to an extended polymer conformation that in turn minimizes the tendency for intramolecular interactions. These results not only provide fundamental insight into mechanisms by which polymers modify nucleation rates, but also pave the way for the rational design of new materials for crystallization inhibition.

ASSOCIATED CONTENT

Supporting Information

The Supporting Information is available free of charge on the ACS Publications website at DOI: 10.1021/acs.biomac.8b01280.

(1) Experimental conditions used in nucleation induction time experiments; (2) reported amorphous and crystalline solubility values for the model drugs; and (3) physicochemical properties of newly synthesized polymers (PDF).

DOI: 10.1021/acs.biomac.8b01280
Biomacromolecules 2018, 19, 4593−4606

AUTHOR INFORMATION

Corresponding Author

*E-mail: lstaylor@purdue.edu. Fax: +1 (765) 494-6545. Tel.: +1 (765) 714-2808.

ORCID

Laura I. Mosquera-Giraldo: 0000-0003-4045-5491
Carlos H. Borca: 0000-0003-0683-7613
Kevin J. Edgar: 0000-0002-9459-9477
Lyudmila V. Slipchenko: 0000-0002-0445-2990
Lynne S. Taylor: 0000-0002-4568-6021

Author Contributions

The manuscript was written through contributions of all authors. All authors have given approval to the final version of the manuscript.

Notes

The authors declare no competing financial interest.

ACKNOWLEDGMENTS

This research was supported in part by a Graduate Student Fellowship Award from the American Association of Pharmaceutical Scientists (AAPS) to L.M. We also express thanks for funding provided by the McKeehan Graduate Fellowship in Pharmacy, and the Migliaccio/Pfizer Graduate Fellowship in Pharmaceutical Sciences, awarded to L.M. We would like to acknowledge the National Science Foundation for their financial support through Grant DMR-1309218. This research was supported in part through computational resources provided by Information Technology at Purdue University.

REFERENCES

(1) Abel, R.; Mondal, S.; Masse, C.; Greenwood, J.; Harriman, G.; Ashwell, M. A.; Bhat, S.; Wester, R.; Frye, L.; Kapeller, R.; Friesner, R. A. Accelerating drug discovery through tight integration of expert molecular design and predictive scoring. *Curr. Opin. Struct. Biol.* **2017**, *43*, 38−44.

(2) Abel, R.; Wang, L.; Harder, E. D.; Berne, B. J.; Friesner, R. A. Advancing Drug Discovery through Enhanced Free Energy Calculations. *Acc. Chem. Res.* **2017**, *50* (7), 1625−1632.

(3) Kapetanovic, I. M. Computer-aided drug discovery and development (CADDD): In silico-chemico-biological approach. *Chem.-Biol. Interact.* **2008**, *171* (2), 165−176.

(4) Durrant, J. D.; McCammon, J. A. Molecular dynamics simulations and drug discovery. *BMC Biol.* **2011**, *9* (1), 71.

(5) Blundell, T. Protein crystallography and drug discovery: recollections of knowledge exchange between academia and industry. *IUCrJ* **2017**, *4* (4), 308−321.

(6) Landis, M. S.; Bhattachar, S.; Yazdanian, M.; Morrison, J. Commentary: Why Pharmaceutical Scientists in Early Drug Discovery Are Critical for Influencing the Design and Selection of Optimal Drug Candidates. *AAPS PharmSciTech* **2018**, *19* (1), 1−10.

(7) Mosquera-Giraldo, L. I.; Borca, C. H.; Meng, X.; Edgar, K. J.; Slipchenko, L. V.; Taylor, L. S. Mechanistic Design of Chemically Diverse Polymers with Applications in Oral Drug Delivery. *Biomacromolecules* **2016**, *17* (11), 3659−3671.

(8) Ilevbare, G. A.; Liu, H.; Edgar, K. J.; Taylor, L. S. Maintaining Supersaturation in Aqueous Drug Solutions: Impact of Different Polymers on Induction Times. *Cryst. Growth Des.* **2013**, *13* (2), 740−751.

(9) Ting, J. M.; Porter, W. W.; Mecca, J. M.; Bates, F. S.; Reineke, T. M. Advances in Polymer Design for Enhancing Oral Drug Solubility and Delivery. *Bioconjugate Chem.* **2018**, *29* (4), 939−952.

(10) Ting, J. M.; Navale, T. S.; Jones, S. D.; Bates, F. S.; Reineke, T. M. Deconstructing HPMCAS: Excipient Design to Tailor Polymer−Drug Interactions for Oral Drug Delivery. *ACS Biomater. Sci. Eng.* **2015**, *1* (10), 978−990.

(11) Ting, J. M.; Navale, T. S.; Bates, F. S.; Reineke, T. M. Design of Tunable Multicomponent Polymers as Modular Vehicles To Solubilize Highly Lipophilic Drugs. *Macromolecules* **2014**, *47* (19), 6554−6565.

(12) Yin, L.; Hillmyer, M. A. Preparation and performance of hydroxypropyl methylcellulose esters of substituted succinates for in vitro supersaturation of a crystalline hydrophobic drug. *Mol. Pharmaceutics* **2014**, *11* (1), 175−85.

(13) Dong, Y.; Mosquera-Giraldo, L. I.; Taylor, L. S.; Edgar, K. J. Amphiphilic Cellulose Ethers Designed for Amorphous Solid Dispersion via Olefin Cross-Metathesis. *Biomacromolecules* **2016**, *17* (2), 454−465.

(14) Dong, Y.; Mosquera-Giraldo, L. I.; Taylor, L. S.; Edgar, K. J. Tandem modification of amphiphilic cellulose ethers for amorphous solid dispersion via olefin cross-metathesis and thiol-Michael addition. *Polym. Chem.* **2017**, *8* (20), 3129−3139.

(15) Liu, H.; Taylor, L. S.; Edgar, K. J. The role of polymers in oral bioavailability enhancement; a review. *Polymer* **2015**, *77*, 399−415.

(16) Jha, P. K.; Larson, R. G. Assessing the Efficiency of Polymeric Excipients by Atomistic Molecular Dynamics Simulations. *Mol. Pharmaceutics* **2014**, *11* (5), 1676−1686.

(17) Maniruzzaman, M.; Pang, J.; Morgan, D. J.; Douroumis, D. Molecular modeling as a predictive tool for the development of solid dispersions. *Mol. Pharmaceutics* **2015**, *12* (4), 1040−9.

(18) Gupta, J.; Nunes, C.; Vyas, S.; Jonnalagadda, S. Prediction of solubility parameters and miscibility of pharmaceutical compounds by molecular dynamics simulations. *J. Phys. Chem. B* **2011**, *115* (9), 2014−23.

(19) Tsvetkov, V.; Serbin, A. A novel view of modelling interactions between synthetic and biological polymers via docking. *J. Comput.-Aided Mol. Des.* **2012**, *26* (12), 1369−1388.

(20) Chodera, J. D.; Mobley, D. L.; Shirts, M. R.; Dixon, R. W.; Branson, K.; Pande, V. S. Alchemical free energy methods for drug discovery: progress and challenges. *Curr. Opin. Struct. Biol.* **2011**, *21* (2), 150−160.

(21) Ahmad, S.; Johnston, B. F.; Mackay, S. P.; Schatzlein, A. G.; Gellert, P.; Sengupta, D.; Uchegbu, I. F. In silico modelling of drug-polymer interactions for pharmaceutical formulations. *J. R. Soc., Interface* **2010**, *7* (Suppl 4), S423−33.

(22) Subashini, M.; Devarajan, P. V.; Sonavane, G. S.; Doble, M. Molecular dynamics simulation of drug uptake by polymer. *J. Mol. Model.* **2011**, *17* (5), 1141−7.

(23) Kasimova, A. O.; Pavan, G. M.; Danani, A.; Mondon, K.; Cristiani, A.; Scapozza, L.; Gurny, R.; Moller, M. Validation of a novel molecular dynamics simulation approach for lipophilic drug incorporation into polymer micelles. *J. Phys. Chem. B* **2012**, *116* (14), 4338−45.

(24) Mackenzie, R.; Booth, J.; Alexander, C.; Garnett, M. C.; Laughton, C. A. Multiscale modeling of drug-polymer nanoparticle assembly identifies parameters influencing drug encapsulation efficiency. *J. Chem. Theory Comput.* **2015**, *11* (6), 2705−13.

(25) Gao, Y.; Olsen, K. W. Drug-polymer interactions at water-crystal interfaces and implications for crystallization inhibition: molecular dynamics simulations of amphiphilic block copolymer interactions with tolazamide crystals. *J. Pharm. Sci.* **2015**, *104* (7), 2132−41.

(26) Katiyar, R. S.; Jha, P. K. Molecular simulations in drug delivery: Opportunities and challenges. *Wiley Interdiscip. Rev.: Comput. Mol. Sci.* **2018**, *8*, e1358.

(27) Borca, C. H.; Arango, C. A. Molecular Dynamics of a Water-Absorbent Nanoscale Material Based on Chitosan. *J. Phys. Chem. B* **2016**, *120* (15), 3754−64.

(28) Karavas, E.; Georgarakis, E.; Sigalas, M. P.; Avgoustakis, K.; Bikiaris, D. Investigation of the release mechanism of a sparingly water-soluble drug from solid dispersions in hydrophilic carriers based on physical state of drug, particle size distribution and drug−polymer interactions. *Eur. J. Pharm. Biopharm.* **2007**, *66* (3), 334−347.

(29) Lima, A. A.; Soares-Sobrinho, J. L.; Silva, J. L.; Correa-Junior, R. A.; Lyra, M. A.; Santos, F. L.; Oliveira, B. G.; Hernandes, M. Z.;

DOI: 10.1021/acs.biomac.8b01280
Biomacromolecules 2018, 19, 4593−4606

Rolim, L. A.; Rolim-Neto, P. J. The use of solid dispersion systems in hydrophilic carriers to increase benzonidazole solubility. *J. Pharm. Sci.* **2011**, *100* (6), 2443−51.
(30) Moghadam, S.; Larson, R. G. Assessing the Efficacy of Poly(N-isopropylacrylamide) for Drug Delivery Applications Using Molecular Dynamics Simulations. *Mol. Pharmaceutics* **2017**, *14* (2), 478−491.
(31) Huang, W.; Mandal, T.; Larson, R. G. Computational Modeling of Hydroxypropyl-Methylcellulose Acetate Succinate (HPMCAS) and Phenytoin Interactions: A Systematic Coarse-Graining Approach. *Mol. Pharmaceutics* **2017**, *14* (3), 733−745.
(32) Meng, X.; Roy Choudhury, S.; Edgar, K. J. Multifunctional cellulose esters by olefin cross-metathesis and thiol-Michael addition. *Polym. Chem.* **2016**, *7* (23), 3848−3856.
(33) Dong, Y.; Edgar, K. J. Imparting functional variety to cellulose ethers via olefin cross-metathesis. *Polym. Chem.* **2015**, *6* (20), 3816−3827.
(34) Dong, Y.; Mosquera-Giraldo, L. I.; Taylor, L. S.; Edgar, K. J. Amphiphilic Cellulose Ethers Designed for Amorphous Solid Dispersion via Olefin Cross-Metathesis. *Biomacromolecules* **2016**, *17*, 454−465.
(35) Meng, X.; Matson, J. B.; Edgar, K. J. Olefin Cross-Metathesis as a Source of Polysaccharide Derivatives: Cellulose ω-Carboxyalkanoates. *Biomacromolecules* **2014**, *15* (1), 177−187.
(36) Meng, X.; Matson, J. B.; Edgar, K. J. Olefin cross-metathesis, a mild, modular approach to functionalized cellulose esters. *Polym. Chem.* **2014**, *5* (24), 7021−7033.
(37) Van Der Spoel, D.; Lindahl, E.; Hess, B.; Groenhof, G.; Mark, A. E.; Berendsen, H. J. C. Gromacs: Fast, Flexible, and Free. *J. Comput. Chem.* **2005**, *26*, 1701−1718.
(38) Hess, B.; Kutzner, C.; van der Spoel, D.; Lindahl, E. GROMACS 4: Algorithms for Highly Efficient, Load-Balanced, and Scalable Molecular Simulation. *J. Chem. Theory Comput.* **2008**, *4* (3), 435−47.
(39) Brooks, B. R.; Bruccoleri, R. E.; Olafson, B. D.; States, D. J.; Swaminathan, S.; Karplus, M. CHARMM: A program for macromolecular energy, minimization, and dynamics calculations. *J. Comput. Chem.* **1983**, *4* (2), 187−217.
(40) MacKerell, A. D.; Banavali, N.; Foloppe, N. Development and current status of the CHARMM force field for nucleic acids. *Biopolymers* **2000**, *56* (4), 257−265.
(41) Froimowitz, M. HyperChem: a software package for computational chemistry and molecular modeling. *Biotechniques* **1993**, *14* (6), 1010−1013.
(42) Zoete, V.; Cuendet, M. A.; Grosdidier, A.; Michielin, O. SwissParam: a fast force field generation tool for small organic molecules. *J. Comput. Chem.* **2011**, *32* (11), 2359−68.
(43) Essmann, U.; Perera, L.; Berkowitz, M. L.; Darden, T.; Lee, H.; Pedersen, L. G. A smooth particle mesh Ewald method. *J. Chem. Phys.* **1995**, *103* (19), 8577−8593.
(44) Still, W. C.; Tempczyk, A.; Hawley, R. C.; Hendrickson, T. Semianalytical treatment of solvation for molecular mechanics and dynamics. *J. Am. Chem. Soc.* **1990**, *112* (16), 6127−6129.
(45) Eisenhaber, F.; Lijnzaad, P.; Argos, P.; Sander, C.; Scharf, M. The double cubic lattice method: Efficient approaches to numerical integration of surface area and volume and to dot surface contouring of molecular assemblies. *J. Comput. Chem.* **1995**, *16* (3), 273−284.
(46) Gelbrich, T.; Kahlenberg, V.; Langes, C.; Griesser, U. J. Telaprevir: helical chains based on three-point hydrogen-bond connections. *Acta Crystallogr., Sect. C: Cryst. Struct. Commun.* **2013**, *69* (2), 179−82.
(47) Kim, S.; Lotz, B. T.; Malley, M. F.; Gougoutas, J. Z.; Davidovich, M.; Srivastava, S. K. *CCDC 954634: Experimental Crystal Structure Determination*; Cambridge Crystallographic Data Centre, 2015.
(48) Shao, Y.; Gan, Z.; Epifanovsky, E.; Gilbert, A. T. B.; Wormit, M.; Kussmann, J.; Lange, A. W.; Behn, A.; Deng, J.; Feng, X.; Ghosh, D.; Goldey, M.; Horn, P. R.; Jacobson, L. D.; Kaliman, I.; Khaliullin, R. Z.; Kuś, T.; Landau, A.; Liu, J.; Proynov, E. I.; Rhee, Y. M.; Richard, R. M.; Rohrdanz, M. A.; Steele, R. P.; Sundstrom, E. J.; Woodcock, H. L.; Zimmerman, P. M.; Zuev, D.; Albrecht, B.; Alguire, E.; Austin, B.; Beran, G. J. O.; Bernard, Y. A.; Berquist, E.; Brandhorst, K.; Bravaya, K. B.; Brown, S. T.; Casanova, D.; Chang, C.-M.; Chen, Y.; Chien, S. H.; Closser, K. D.; Crittenden, D. L.; Diedenhofen, M.; DiStasio, R. A.; Do, H.; Dutoi, A. D.; Edgar, R. G.; Fatehi, S.; Fusti-Molnar, L.; Ghysels, A.; Golubeva-Zadorozhnaya, A.; Gomes, J.; Hanson-Heine, M. W. D.; Harbach, P. H. P.; Hauser, A. W.; Hohenstein, E. G.; Holden, Z. C.; Jagau, T.-C.; Ji, H.; Kaduk, B.; Khistyaev, K.; Kim, J.; Kim, J.; King, R. A.; Klunzinger, P.; Kosenkov, D.; Kowalczyk, T.; Krauter, C. M.; Lao, K. U.; Laurent, A. D.; Lawler, K. V.; Levchenko, S. V.; Lin, C. Y.; Liu, F.; Livshits, E.; Lochan, R. C.; Luenser, A.; Manohar, P.; Manzer, S. F.; Mao, S.-P.; Mardirossian, N.; Marenich, A. V.; Maurer, S. A.; Mayhall, N. J.; Neuscamman, E.; Oana, C. M.; Olivares-Amaya, R.; O'Neill, D. P.; Parkhill, J. A.; Perrine, T. M.; Peverati, R.; Prociuk, A.; Rehn, D. R.; Rosta, E.; Russ, N. J.; Sharada, S. M.; Sharma, S.; Small, D. W.; Sodt, A.; Stein, T.; Stück, D.; Su, Y.-C.; Thom, A. J. W.; Tsuchimochi, T.; Vanovschi, V.; Vogt, L.; Vydrov, O.; Wang, T.; Watson, M. A.; Wenzel, J.; White, A.; Williams, C. F.; Yang, J.; Yeganeh, S.; Yost, S. R.; You, Z.-Q.; Zhang, I. Y.; Zhang, X.; Zhao, Y.; Brooks, B. R.; Chan, G. K. L.; Chipman, D. M.; Cramer, C. J.; Goddard, W. A.; Gordon, M. S.; Hehre, W. J.; Klamt, A.; Schaefer, H. F.; Schmidt, M. W.; Sherrill, C. D.; Truhlar, D. G.; Warshel, A.; Xu, X.; Aspuru-Guzik, A.; Baer, R.; Bell, A. T.; Besley, N. A.; Chai, J.-D.; Dreuw, A.; Dunietz, B. D.; Furlani, T. R.; Gwaltney, S. R.; Hsu, C.-P.; Jung, Y.; Kong, J.; Lambrecht, D. S.; Liang, W.; Ochsenfeld, C.; Rassolov, V. A.; Slipchenko, L. V.; Subotnik, J. E.; Van Voorhis, T.; Herbert, J. M.; Krylov, A. I.; Gill, P. M. W.; Head-Gordon, M. Advances in molecular quantum chemistry contained in the Q-Chem 4 program package. *Mol. Phys.* **2015**, *113* (2), 184−215.
(49) Ernzerhof, M.; Scuseria, G. E. Assessment of the Perdew−Burke−Ernzerhof exchange-correlation functional. *J. Chem. Phys.* **1999**, *110* (11), 5029−5036.
(50) Adamo, C.; Barone, V. Toward reliable density functional methods without adjustable parameters: The PBE0 model. *J. Chem. Phys.* **1999**, *110* (13), 6158−6170.
(51) GROMACS development team; http://manual.gromacs.org/documentation/2018/onlinehelp/gmx-energy.html.
(52) Dong, Y.; Matson, J. B.; Edgar, K. J. Olefin Cross-Metathesis in Polymer and Polysaccharide Chemistry: A Review. *Biomacromolecules* **2017**, *18* (6), 1661−1676.
(53) Schram, C. J.; Beaudoin, S. P.; Taylor, L. S. Impact of Polymer Conformation on the Crystal Growth Inhibition of a Poorly Water-Soluble Drug in Aqueous Solution. *Langmuir* **2015**, *31* (1), 171−179.
(54) Fedors, R. F. A method for estimating both the solubility parameters and molar volumes of liquids. *Polym. Eng. Sci.* **1974**, *14* (2), 147−154.
(55) Lu, J.; Ormes, J. D.; Lowinger, M.; Mann, A. K. P.; Xu, W.; Litster, J. D.; Taylor, L. S. Maintaining Supersaturation of Active Pharmaceutical Ingredient Solutions with Biologically Relevant Bile Salts. *Cryst. Growth Des.* **2017**, *17* (5), 2782−2791.
(56) Indulkar, A. S.; Gao, Y.; Raina, S. A.; Zhang, G. G. Z.; Taylor, L. S. Crystallization from Supersaturated Solutions: Role of Lecithin and Composite Simulated Intestinal Fluid. *Pharm. Res.* **2018**, *35* (8), 158.
(57) Gniado, K.; Lobmann, K.; Rades, T.; Erxleben, A. The influence of co-formers on the dissolution rates of co-amorphous sulfamerazine/excipient systems. *Int. J. Pharm.* **2016**, *504* (1−2), 20−6.
(58) Dong, Y.; Mosquera-Giraldo, L. I.; Troutman, J.; Skogstad, B.; Taylor, L. S.; Edgar, K. J. Amphiphilic hydroxyalkyl cellulose derivatives for amorphous solid dispersion prepared by olefin cross-metathesis. *Polym. Chem.* **2016**, *7* (30), 4953−4963.
(59) de Araujo, G. L.; Benmore, C. J.; Byrn, S. R. Local Structure of Ion Pair Interaction in Lapatinib Amorphous Dispersions characterized by Synchrotron X-Ray diffraction and Pair Distribution Function Analysis. *Sci. Rep.* **2017**, *7*, 46367.
(60) Maniruzzaman, M.; Snowden, M. J.; Bradely, M. S.; Douroumis, D. Studies of intermolecular interactions in solid dispersions using advanced surface chemical analysis. *RSC Adv.* **2015**, *5* (91), 74212−74219.
(61) Vekilov, P. G. The two-step mechanism of nucleation of crystals in solution. *Nanoscale* **2010**, *2* (11), 2346−2357.
(62) Anwar, J.; Boateng, P. K.; Tamaki, R.; Odedra, S. Mode of Action and Design Rules for Additives That Modulate Crystal Nucleation. *Angew. Chem., Int. Ed.* **2009**, *48* (9), 1596−1600.

DOI: 10.1021/acs.biomac.8b01280
Biomacromolecules 2018, 19, 4593−4606